Land subsidence along the Ionian coast of SE Sicily (Italy), detection and analysis via Small Baseline Subset (SBAS) multitemporal differential SAR interferometry.

Fabio Canova,[1*] Cristiano Tolomei,[2] Stefano Salvi,[2] Giovanni Toscani,[1] Silvio Seno[1]

[1] Dipartimento di Scienze della Terra e dell'Ambiente, Università degli Studi di Pavia, Pavia, Italy

[2] Istituto Nazionale di Geofisica e Vulcanologia, Roma, Italy

[*]Correspondence to: Fabio Canova, Dipartimento di Scienze della Terra e dell'Ambiente, Università degli studi di Pavia, Via Ferrata, n°1, 27100 - Pavia, Italy.

Tel: ++390382985846 - E-mail: fabio.canova@dst.unipv.it

ABSTRACT: We present the results of a multi-temporal, differential interferometric synthetic aperture radar (DInSAR) analysis aiming to identify active surface deformation phenomena in southeastern Sicily. The study area has been chosen because of its strong seismicity, high concentration of industrial and agricultural activities, and high density of people living in the coastal area. Furthermore, the morphology, lithology and climatic feature of this sector of the Hyblean foreland are suitable for an interferometric analysis, providing a high coherence over the area.

We used the Small BAseline Subset (SBAS) multitemporal DInSAR technique from Berardino *et al.*, 2002, to calculate mean ground velocity maps and displacement time series from a large data set of European Remote Sensing Satellites (ERS 1-2) images spanning the time period 1992-2000.

The reliability of the DInSAR results was tested calculating the $East_{SAR}$ and Up_{SAR} values over two permanent global positioning system (GPS) stations in the area, and comparing them with the $East_{GPS}$ and Up_{GPS} values. The residuals between GPS and DInSAR velocities were 1 and 0.6 mm/yr for the Up and East components, respectively. Four main subsiding areas, previously undetected, have been identified, in correspondence of the towns of Augusta, Siracusa, Priolo, and Villasmundo. The observed deformation phenomena are located within coastal structural basins, filled with Pleistocene and Holocence deposits, except the Villasmundo land subsidence which is located on the Hyblean

plateau. The measured deformation rates reach values up to -18 mm/yr in Augusta, -6 mm/yr in Siracusa, -5 mm/yr in Villasmundo and -4.5 mm/yr in Priolo. The examination of velocity profiles, time series, and geological data allows us to relate all the detected deformation patterns primarily to groundwater over-exploitation. A multi-dimensional interpolation with kriging was performed to obtain a field subsidence map. A first order elastic deformation model was used to simulate the peculiar features of the Villasmundo subsidence.

KEYWORDS: Subsidence, Radar Interferometry, south-eastern Sicily, SBAS, aquifer-system compaction

Introduction

Land subsidence consists in the gradual settling or sudden sinking of the topographic surface, and may be triggered by natural processes, such as compaction of sediments, or by anthropogenic ones, like groundwater, oil and fluid extraction, or mining (Galloway *et al.*, 1999). The strong exploitation of these natural resources in the past half-century has caused a dramatic acceleration of subsidence rates in several areas around the world (Strozzi *et al.*, 2001). For example, in the United States, more than 44,000 square kilometres of land have been directly affected by subsidence, 80% of which is attributed to human impact on subsurface water and overexploitation of groundwater resources (Galloway *et al.*, 1999). It has been reported that in 1995 more than 150 major cities in the world suffered serious problems of subsidence due to excessive ground-water withdrawal (Hu *et al.*, 2004). The economical, social and environmental impact of anthropogenic land subsidence has long been recognized by scientific institutions and local authorities and land subsidence is among the research issues recommended by the United Nations Educational, Scientific and Cultural Organization (UNESCO) in the framework of the International Hydrological Decades (IHD) since 1965 (Barends *et al.*, 1995).

Three distinct processes account for most water-related anthropogenic subsidence: compaction of aquifer systems, drainage and subsequent oxidation of organic soils, and dissolution and collapse of susceptible rocks. Compaction of unconsolidated aquifer systems is by far the single largest cause of subsidence (Galloway *et al.*, 1999).

The compression of an artesian aquifer following an artesian head decline was described primarily by Meinzer and Hard (1925). They stated that the overburden pressure of all beds above the confined aquifer is partly supported by the fluid pressure at the top of the aquifer and partly by the aquifer grain-to-grain load, concluding that all artesian aquifers are apparently more or less compressible and elastic,

especially those with low permeability, small recharge and high head. Later Jacob (1940) postulated that when water is removed from an elastic artesian aquifer and pressure is decreased, stored water is derived by compression of the aquifer and of the adjacent and included clay beds. To describe primary one-dimensional clay consolidation we have to refer to Terzaghi's principle of effective stress (Terzaghi, 1925). According to this theory, compaction results from the slow escape of pore water from the stressed deposits, accompanied by a gradual transfer of stress from the pore water to the granular structure of the deposits. The application of Terzaghi soil consolidation theory to aquifer-system compaction was summarized by Riley (1969) who stated that the consolidation of a multi-layered aquifer system in response to an increase of applied stress is strongly time dependent because of the low permeability and relatively high compressibility of interbedded aquitards.

The consolidation process of multi-layered aquifer systems due to groundwater overdraft can result in dramatic peaks of subsidence. Among the most striking examples we can cite the Mexico city case, 9 meters of vertical deformation over an area of 225 km^2 between 1891 and 1978 in alluvial and lacustrine deposits (Marsal and Mazari, 1959; Figueroa-Vega, 1984) and the San Joaquin Valley (California) aquifer system compaction, 9 meters of subsidence between 1930 and 1975 over an area of 6200 km^2 also in alluvial and lacustrine deposits (Poland, 1975).

Although most of the subsidence cases involve unconsolidated or poorly consolidated aquifer systems, the production of gas, oil and water can trigger subsidence phenomena even in consolidated-rock reservoirs. Reservoir compaction is governed by three main parameters: increasing of effective stress (i.e. pore pressure decline after production onset), reservoir thickness and reservoir rock compressibility. The reservoir pressure depletion can result in land sinking and seabed subsidence, and ground ruptures (earth fissures or activation of surface faults) resulting in damages to wells and other built infrastructures. Among the most cited examples is the West Ekofisk field in the North Sea, where compaction of the chalk reservoir, after a 300% increase in effective stress, produced nearly 8 meters of seabed subsidence. This led to jacking of the platform in 1987, placement of barriers in 1989, and the Ekofisk II redevelopment in 1998 (Nagel, 2001 and references therein).

Traditionally, the measurement of land subsidence was carried out using precision levelling surveys, GPS (continuous or survey-mode) and extensometer wells. In the last two decades, the development of Differential Interferometric Synthetic Aperture Radar (DInSAR) techniques has provided a new way for low-cost, time-effective, and precise ground deformation monitoring. DInSAR is a space-based technique that allows the detection and measurement of ground deformation over large areas exploiting phase differences between successive radar acquisitions (Castañeda *et al.*, 2009). The most important,

and unique, advantage of DInSAR is the capacity to yield spatially and temporally dense measurements, resulting in impressive scientific advances in different geological and geophysical fields, such as seismology, volcanology, glacier dynamics, active landslide deformations and land subsidence (Bürgmann *et al.*, 2000). Outstanding results have been achieved in hydrogeology, where the integration of SAR data, geologic information and groundwater levels, have allowed the constraining of parameters estimates in simulations of aquifer system compaction (Galloway *et al.*, 1998; Galloway and Hoffmann, 2007). In the last ten years, several techniques, that allow the generation of time series have been proposed, first using conventional DInSAR (Amelung *et al.*, 1999; Hoffmann *et al.*, 2003), and then using multitemporal (or time-series) DInSAR techniques (PSInSAR, Ferretti *et al.*, 2001; SBAS, Berardino *et al.*, 2002; IPTA, Wegmuller *et al.*, 2004; STAMPS, Hooper *et al.*, 2004; CPT, Blanco-Sanchez *et al.*, 2008), which exploit the inversion of an appropriate sequence of DInSAR interferograms to generate time series and monitor the temporal evolution of the detected phenomena (Lanari *et al.*, 2007).

In this study we measured ground deformation rates in southeastern Sicily via the Small BAseline Subset (SBAS) technique for time-series DInSAR (Berardino *et al.*, 2002) using image data from the European Remote Sensing Satellites (ERS 1-2) spanning the time period 1992-2000. The ERS 1-2 sensors have a revisiting time of 35 days and operate at C-band (5.33 GHz central frequency corresponding to a 5.65 cm wavelength), this implies that temporal decorrelation, creating noise in the DInSAR interferograms, is highly dependent on the land covers. Urban and vegetation-free areas are the most suitable surfaces, while areas affected by agricultural practice, erosion and aggradation, are the least suitable (Castañeda *et al.*, 2009).

Unlike Persistent Scatterers (PS-InSAR, IPTA, STAMPS) approaches, which only analyze stable radar reflectors consisting of single targets unaffected by temporal and spatial decorrelation, Small Baseline (SB) methods (Lundgren *et al.*, 2001; Berardino *et al.*, 2002; Mora *et al.*, 2003; Schmidt and Burgmann, 2003; Prati *et al.*, 2010) detects also distributed scatterers, maximizing the coherent pixels density. This is obtained using an appropriate combination of averaged (multi-look) differential interferograms, characterized by relatively small orbital (spatial) and temporal separations of the SAR images, as well as by a small frequency shift in the doppler centroids (Franceschetti and Lanari, 1999) in order to reduce the decorrelation effects (Castañeda *et al.*, 2009). In the SBAS algorithm, this task is achieved grouping SAR image pairs in one or more small baseline subsets, that are appropriately linked using the Singular Value Decomposition (SVD) method to retrieve the deformation time series. Another peculiarity of the SBAS algorithm is the possibility to investigate large spatial scale

displacement with relatively low resolution (e.g. 160 x160 m), as shown recently by Casu *et al.*, 2008 who applied the SBAS to long SAR image strips (600x100 km). The SBAS has been successfully applied to analyze surface deformation effects relevant to different phenomena: deformation in volcanic areas (Lanari *et al.*, 2004a; Lundgren *et al.*, 2004; Borgia *et al.*, 2005; Manzo *et al.*, 2006; Tizzani *et al.*, 2007), deformation due to fluid withdrawal (Lanari *et al.*, 2004b), tectonic activity (Hunstad *et al.*, 2009; Guzzetti *et al.*, 2009), mining subsidence (Baek *et al.*, 2008), urban area deformations (Lanari *et al.*, 2004c; Cascini *et al.*, 2006), with the potential to discriminate between the natural and anthropogenic components of deformation (Stramondo *et al.*, 2007).

In this study, we performed a detailed survey of the land subsidence occurring in the coastal area of southeastern Sicily, a region highly prone to seismic (DISS Working Group, 2010) and environmental hazards, whose most prominent feature is the Hyblean plateau, representing the on land foreland portion of the Maghrebian fold-and-thrust belt section exposed in Sicily. The largest historical earthquake ever happened in Italy struck this region in 1693, followed by a devastating tsunami recorded along the whole coast of eastern Sicily (Bianca *et al.*, 1999 and references therein). The most recent damaging event (M_L 5.4, 12/13/1990), located 20 km offshore Augusta, caused 19 victims and severe damages to buildings and infrastructures (Amato *et al.*, 1995), due to important site amplifications in lowland areas (Decanini and Panza, 2000). The area is also the site of a large chemical industrial park whose main activities are: refinement, storage, and moving of crude oil, production of chemical compounds, cement, technical gases, and electricity. Intensive agricultural practice is widespread too, as well as residential housing, mainly along the coastal area.

Geological and hydrogeological setting of southeastern Sicily

The study area lays on the southeastern part of Sicily, along the Ionian coast, between Augusta and Siracusa (Fig. 1). The most peculiar morphological feature in this sector is the Hyblean plateau, a prominent horst-like peripheral bulge structure, dissected by several normal and strike slip fault systems limiting minor horsts and grabens (Ghisetti and Vezzani, 1980). The Hyblean plateau represents the Tertiary orogenic foreland of the Maghrebian thrust-fold belt, and shows sharp boundaries with the adjacent crustal units (Ben-Avraham and Grasso, 1991). To the northwest it is separated by a narrow foredeep, extending from Catania to Gela, from the "Gela Nappe", the Plio-Pleistocene external front of the Maghrebian thrust belt. To the southwest, it is bounded by the NNE-SSW Scicli-Ragusa transcurrent fault system. Eastward it is bounded by the Malta Escarpment, an

inherited Mesozoic tectonic boundary that separates the continental crust of the Hyblean plateau from the Ionian oceanic crust (Scandone, 1981; Ben-Avraham and Grasso, 1991; Grasso, 1993).

The Hyblean sequence mainly comprises a Meso-Cenozoic carbonates succession deposited in platform facies with several volcanic horizons that occurred intermittently from late Triassic through early Pleistocene (Bianchi, 1987; Lentini, 1987). Because of their huge extension, coupled with high permeability values, carbonate rocks and volcanic deposits constitute very important regional aquifers.

Along the Ionian coast, at the onset of the Pleistocene (Adam *et al.*, 2000), the secondary faults of the Malta Escarpment controlled the development of an array of minor basins, arranged in a Graben-Horst pattern (Grasso *et al.*, 1993). From North to South calcareous ridges bound the Augusta, Marcellino, Priolo and Anapo grabens. Along the master faults of the grabens, the vertical offset increases eastward, approaching the Malta Escarpment and the sea (Adam *et al.*, 2000). This morphology favoured the development of the coastal cities and harbours: the grabens provide the appropriate sea-bottom depth, while the isolated and discontinuous ridges made by upper Miocene limestone and calcarenites shelter the gulfs from winds and waves. Inside these coastal grabens, over the Meso-Cenozoic sequence, lie the Quaternary deposits. The succession starts with lower Pleistocene yellowish calcarenites and sands (Qc, Fig. 2), poorly cemented and medium to fine grained, with polygenic conglomerates layer and silty lagoon clay lenses at the base. Those sediments often onlap above the Plio-Pleistocene lavas paleosurface. These calcarenites and sands grade up and laterally to a monotone sequence of over-consolidated (over-consolidated ratio, OCR= 2.0 to 6.0, from Lo Presti *et al.*, 1998), medium stiff, marine, blue clays (Qa, blue-clays, lower Pleistocene), with low to medium plasticity index (P.I.). Those sediments, in the Augusta bay area, reach a maximum thickness of more than 300 meters. On top, separated from the blue clays by another unconformity, lie the biocalcarenites of middle Pleistocene (Carbone, 1985), covered by sands, calcarenites and conglomerates of Tyrrhenian age (Qs, Fig. 2), with *Strombus Bubonius*. Recent alluvial deposits of gravel, sands, and clays of Holocene age close the stratigraphic sequence. All the layers dip toward E or ENE at angles between 0° and 10°.

In the coastal area, the afore-mentioned blue-clay lower Pleistocene deposits (Qa) separate two main aquifers (Fig. 2). The upper one is an unconfined aquifer of small thickness and scarce productivity, represented by alluvial deposits (hydraulic conductivity, K 10^{-3} - 10^{-5} cm/s), coarse to fine grained sands and yellowish biogenic calcarenites (Qs, K $10^{-2} \div 10^{-3}$ cm/s), with cross stratification, often terraced at the top. It is intensely exploited, and often connected with the lower aquifers-system through intraborehole flow in numerous inadequately isolated boreholes (Aureli *et al.*, 1987c). The

lower aquifer system can be divided in three sub-units (Fig. 2): a first one made by the upper Cretaceous to Tortonian calcareous and calcarenitic deposits (M) with low to high secondary permeability, depending on the amount of fractures and on the presence of karst caves. The second and third sub-units lie above the calcareous bedrock, the former being represented by effusive rocks, massives or pyroclastic (Pv, K $10^{-2} \div 10^{-4}$ cm/s), with different degree of alteration and the latter by poligenic conglomerates, calcarenites and sand (Qc, K $10^{-2} \div 10^{-3}$ cm/s) with high primary permeability (Aureli *et al.*, 1987c).

This aquifer system is unconfined except for the coastal area, where it is confined by the blue clays. It represents the main source for municipal-industrial water supply for Augusta, Siracusa and Priolo aqueducts. In these areas the aquifer system originally showed a high hydraulic head that started to decline in the 1980s due to overexploitation and small recharge, with a maximum hydraulic head decline of -100 meters with respect to the original static level (Aureli *et al.*, 1987a; Aureli *et al.*, 1987b, Aureli *et al.*, 1987c).

Ground velocity estimates by time-series DInSAR

In the 1990s, radar interferometry, revealed an extraordinary potential in the measurements of crustal deformations and was widely used as a new, powerful geodetic technique. This technique exploits carefully engineered differences between spaceborne Synthetic Aperture Radar (SAR) images, acquired with a difference of position or with a difference of time. The phase of images is compared after proper image co-registration. The resulting difference of phases is a new kind of image, called interferogram, an interference pattern of fringes containing all the information on relative geometry (Massonet and Feigl, 1998). There are many physical phenomena contributing to phase measurements: phase variations within a pixel, the contribution of orbital variations, topography, atmosphere, and displacement. The topographic, orbital, and atmospheric contributions are removed in order to reveal ground displacements along the line of sight between the radar and the target.

The DInSAR has been applied several times to the analysis of single deformation episode, generating large-scale surface deformation maps (Massonet and Feigl, 1998). The following aim was to study the temporal evolution of the detected deformations. Several different approaches have been proposed in the last decade to generate time series of ground displacement, first using conventional DInSAR (Amelung *et al.*, 1999; Hoffmann *et al.*, 2003), and then advanced DInSAR techniques: among these the Permanent Scatterers technique (PSInSAR, Ferretti *et al.*, 2001), the Coherent Pixel Technique (CPT, Blanco-Sanchez *et al.*, 2008), the Interferometric Point Target Analysis technique (IPTA,

Wegmuller at al., 2004), and the STanford Method for Persistent Scatterers (STAMPS, Hooper *et al.*, 2004). Most of these methods calculate the displacement time series on point-like targets that exhibit sufficiently high coherence values through time (Persistent or Permanent scatterers).

The SBAS algorithm from Berardino et al. (2002), on the contrary, belongs to the category of advanced DInSAR approaches referred to as Small Baseline (SB) methods. These methods (Lundgren *et al.*, 2001; Berardino *et al.*, 2002; Mora *et al.*, 2003; Schmidt and Burgmann, 2003; Prati *et al.*, 2010) use distributed targets to retrieve deformation time series. The SBAS algorithm combines the acquisitions included in different interferometric subsets using a minimum norm criteria combination of the velocity deformation, based on the Singular Value Decomposition (SVD) method. The SBAS method is able to provide deformation maps with a lower resolution (few tens of meters) than the Persistent or Permanent Scatterers techniques, but with equivalent precision levels (Casu *et al.*, 2006). We refer the reader to Lanari *et al.*, 2007 (and references therein) for a complete description of the SBAS DInSAR technique.

The SAR dataset analyzed in this work comprises 118 ERS images from 1992 to 2000, of which 70 and 48 images were acquired from descending and ascending orbits, respectively. Two hundred interferograms were derived from the descending orbit dataset and 136 were derived from the ascending orbit dataset. To limit coherence losses (i.e. noise), only the interferograms whose image pairs had spatial and temporal baselines less than 200 m and 1200 days, respectively, and doppler centroid differences below 1000 Hz, have been selected. The external DEM used to remove the topographic component from the interferometric phase has a resolution of 80 x 80 meters and was taken by the SRTM NASA mission. Only the pixels where coherence is above a certain threshold (>0.65) were sorted and used.

During the SBAS processing the estimation and removal of temporally decorrelated atmospheric artefacts is performed using a double-pass filtering in the temporal and spatial domains, as explained in Berardino *et al.*, 2002.

The inspection of the final Line of Sight (LoS) mean velocity maps highlighted a possible ramp affecting the ascending map, possibly deriving from imprecise orbital data. Using a first order polynomial regression, after masking all the marked local anomalies, we estimated a small ramp of 0.15 mm/yr/km, which we eventually removed from the map.

From the LoS mean velocity maps we calculated the Up and East components (Fig. 3a, 3b), using the method described in Wright *et al.*, 2004. To validate and check the reliability of the DInSAR ground velocities, we compared them to the East and Up components at the CGPS stations HAGA and SSYX (Devoti *et al.*, 2010). The residuals between the baselines of the GPS and DInSAR velocities between

the HAGA and SSYX sites are 1 mm/yr and 0.6 mm/yr for the Up and East components, respectively. In a comprehensive assessment of the SBAS performance on a comparable ERS dataset carried out by Casu *et al.*, 2006, comparing SBAS mean LoS velocities to several tens of CGPS velocities from the Los Angeles basin, a standard deviation of 1 mm/yr has been found. Since the lack of a dense network of continuous GPS stations did not allow us to make a detailed and independent accuracy assessment all over our area, in agreement with Casu *et al.*, 2006 and Wright *et al.*, 2004, we assume an average standard deviation of ~1 mm/yr for the Up component, and about double for the East component.

Finally, because the deformation of the ground surface is strongly correlated in space and time, we decided to perform a multi-dimensional interpolation with Kriging to obtain a local subsidence map, in order to present the results on a full regular grid (Fig. 6).

Land subsidence observations

The ground velocity map of the Up component shows clear deformation patterns (Fig. 3a). Three main areas affected by localized subsidence, up to -18 mm/yr, can be identified: the Villasmundo area (hereinafter VS), the Augusta - Priolo Gargallo areas (AU and PR), the Siracusa area (SR). In the following we describe the main characteristics of each area.

VS: near the village of Villasmundo the observed land subsidence shows a nearly circular pattern (Fig. 4), with a total E-W extent across the subsiding area of ~3.5 km, and of ~3 km along the N-S. The subsidence pattern shows a circular symmetry in the inner part with maximum rates of -5 mm/yr, and a limited asymmetry in the outer part. As shown in the cross sections (Fig. 4) the ground velocity gradient is smaller to the south and to the west with respect to the northeastern sector. At VS the local stratigraphy shows (from top to bottom) a ~180 m-thick cover of Plio-Quaternary volcanics (basalts), overlying Tortonian volcanoclastic deposits of highly variable thickness, and a bottom unit comprising Tertiary limestones. Both the Plio-Quaternary volcanics and the Tertiary limestones are water-bearing and currently exploited by a high number of wells for municipal water supply. The volcanic deposits show alteration and argillification phenomena, which become more intense and pronounced in the Tortonian volcanoclastic deposits, which locally represent a middle semiconfining unit, sustaining local perched water tables (Aureli *et al.*, 1987c). The subsidence-affected area is located on a gentle, SE-verging slope dissected by two entrenched streams.

AU: we observe significant land subsidence within the Augusta graben. The latter is a structural basin elongated in the NW direction, formed in the last 2-3 million years (Carbone, 1985). The basin is limited to the NE by the Mt. Tauro horst, and is separated from the River Marcellino graben to the SW

by the Petraro horst (Fig. 1). The local stratigraphy shows (Fig. 2) in the first few tens of meters, alluvial and shallow water Holocene deposits (10-20 m), overlying middle Pleistocene calcarenites (Qs, 5-10 m). These units represent the upper aquifer, separated from the lower aquifer system by the underlying lower Pleistocene blue clays (Qa, Fig 2). The intensively exploited lower aquifer system comprises, from top to bottom: lower Pleistocene calcarenites, Plio-Quaternary lavas and Tortonian Volcanoclastics, and Tertiary carbonates. The deformation pattern shows an elongated shape with a NW-SE major axis, parallel to the graben's maximum extent. The subsiding area shows a sharp boundary along the eastern margin, marked by the linear escarpment of the Mt. Tauro fault, and a gentler deformation gradient along the western boundary (Fig. 5). Overall, the subsidence area is ~8.5 km-long (NW-SE) and ~4 km-wide, and shows a mean ground velocity of -6 mm/yr. Strong deformations occur along a NW-SE alignment, parallel to the Mt. Tauro fault, with the largest rates (up to -18.0 mm/yr) located near the new developments of the Augusta urban area, built over reclaimed saltworks (Contrada Saline, Fig. 5). The stable ground surrounding the Augusta (and Marcellino) subsiding areas are mainly based on Tertiary limestones, but also on Plio-Quaternary sediments (e.g. in the River Marcellino graben).

PR: the subsidence measured near Priolo shows a roughly squared shape, insisting in the River Marcellino Graben (Figs. 1, 3a). The dense pattern of pixels (~40 pixel/km^2) is provided by the high numbers of manmade structures located inside the Priolo petrochemical plant. The measured deformation rates are significantly less than those recorded in AS and VS: the mean values is -1.5 mm/yr. A small number of pixels shows subsidence values larger than -3 mm/yr, reaching -4.5 mm/yr above the loading wharfs. The local stratigraphy is the same described in the Augusta area, but in the Marcellino graben the lower Pleistocene blue clays show considerably smaller thickness, reaching maximum values of ~50 meters along the coast, diminishing to zero westward.

SR: proceeding southward, another deformation pattern is located inside the river Anapo graben, west of Siracusa. The subsidence area exhibits a semi-circular shape with the larger values, as much as -6 mm/yr, located along the coast. The whole area has a ~2.5 km extent in a NNE-SSW directions and ~2 km in the NNW-SSE directions. The stratigraphy is similar to the previously described ones, typical of these coastal graben, except for the absence of the Plio-Quaternary volcanic rocks.

Discussion

The most striking feature concerning all the detected subsidence areas but VS is the almost perfect match between their extent and the geometry of the Quaternary basins (Fig. 6). The contour maps

obtained interpolating the DInSAR velocities with a kriging algorithm, excellently fit the geological map with unexpected details (Fig. 6). This is particularly evident in the Augusta and the River Anapo grabens where the subsiding areas actually outline the Quaternary basins flanked by the stable horsts.

The same correspondence between Pleistocene sediments and subsidence is detectable on the PR and SR areas. The Villasmundo subsidence area, however, does not show this correlation, presumably because it is located on Plio-Pleistocene volcanites.

The AU deformation pattern is well aligned with the major axis of the Augusta graben, and the vertical deformation rates gradually increase towards the southeast (see Fig 5, Up velocity on the A-A' profile). The observed deformations are probably related to two different processes.

The first is the compaction of the graben fine grained deposits due to intensive groundwater extraction from the lower aquifer system for industrial, agricultural, and municipal water supply. In the Augusta graben there are many wells, some of them, as much as 400 meters deep, are equipped with 80 l/s delivery capacity pumps. Subsidence due to groundwater overexploitation and piezometric head decline, in the Augusta area, was postulated in the middle 1980s (Aureli *et al.*, 1985, Aureli *et al.*, 1987c), but went undetected, because no detailed vertical deformations measurements were available. As reported in Aureli *et al.*, 1987c, in the Augusta-Priolo area during the 1980's, the static level lowering in the deep aquifer reached 100 meters (not specified the period of reference), with peak values of 150 meters for the dynamic level, bringing the static level close to 100 meters below sea level. Only the occurring of Qa, increasing in thickness seaward, prevented massive saline intrusion, that was only limited to the horst bounding the Quaternary basin and touching the sea, but yet enough to make some wells unusable. The head decline gradually spread and in the western part, where the aquifer is unconfined, many springs disappeared or reduced their discharge, while rivers changed from groundwater draining to groundwater feeding (Aureli *et al.*, 1987c). In the eastern part, where the aquifer is confined by the lower Pleistocene blue clays, the head decline triggered drainage and consolidation phenomena in the confining clays, thus producing subsidence (Aureli *et al.*, 1987c).

The subsidence phenomena ongoing in the Augusta area can be specifically attributed to the compaction of the softest and weakest layer, such as the bottom member of the Lower Pleistocene calcarenites and sands (Qc, Fig.2), which includes clayey-marl and marly-clayey lenses. It seems unlikely that subsidence could be provoked by compaction of the lower Pleistocene blue clays, because they are over-consolidated, medium stiff and their compressibilities decrease with depth, showing an increasing degree of consolidation. (Lo Presti *et al.*, 1998).

The second process, responsible for the largest peaks of subsidence recorded in the Contrada Saline area, is related to the increased load of structures built during the 1980s over poorly consolidated Holocene sediments and reclaimed land, represented by filling material, grey silty clay and silty sands (Lo Presti *et al.,* 1998). The largest rates observed here can neither be attributed to a stronger exploitation of the water table, nor to a greater thickness of the deposits. The superimposition of the two different processes in the Contrada Saline area, and the role played by loading is evident in the ground displacement time series sampled here (time series n°1, Fig. 7) with respect to other displacement time series. In this case, the curve shows a typical transient consolidation trend of exponential decay, compared with the other sites where the trend is almost linear (Fig. 7). Moreover, the high deformation rates characterizing the first period, up to 1997, slow down in the final part of the curve, implying that the deposits are close to complete consolidation. The analysis of time series, velocity profiles and previous data, points out a key role of the massive development that occurred in the Contrada saline area, coupled with the poor geotechnical properties of the soil foundation. The largest mean subsidence rates (-11 mm/yr) correspond to the more recent developments which include closely packed buildings around which the subsidence velocities rapidly decrease with a radial pattern. The soft nature of those sediments has been responsible for the strong site amplification phenomena observed in Contrada Saline during the 1990 earthquake, resulting in serious damages even to reinforced concrete buildings, and liquefaction phenomena of the infilling material of salt works (Decanini and Panza, 2000). In this area several tightly packed buildings, five or six floors high, were built during the middle 1980s; their foundations rest on 25 meter deep, 0.5 meter wide piles (Decanini and Panza, 2000). Decanini and Panza, (2000), obtained seismo-stratigraphic models of the Augusta graben, sampling four sites, two of whom in the Contrada Saline area: the first one was located near the closely packed buildings and the second one was in a not developed area with comparable stratigraphy, close to the sea. They used the Frequency Time ANalysis (FTAN) technique (Dziewonsky *et al.,* 1969; Levshin *et al.,* 1972), and inverted the results using the Hedgehog non-linear method (Valyus *et al.,* 1968; Panza, 1981). The seismo-stratigraphic model obtained nearby the closely packed buildings shows slightly larger (160 m/s) Vs velocities with respect to the undeveloped Contrada Saline site (120 m/s), in the first 10 meters. Decanini and Panza, 2000 ascribed the larger Vs velocities to compaction caused by the group of buildings, the railway, and a viaduct.

It is noteworthy that the maximum subsidence rate of -18 mm/yr is observed in a salt-works area that was infilled in 1991, after the Augusta earthquake, in order to build a temporary shelter camp for evacuated people, but this peak value is limited to a very small sector. Unfortunately, the absence of

piezometric data from the deep aquifer for the time period of interest, and the paucity of geotechnical data at depth prevent us from differentiating the contribution of the two processes.

In the AU area, significant westward horizontal movements are also visible (Figure East) with differential movements of up to 3 mm/yr (profile A-A' in fig 5). These movements do not only occur over the alluvial deposits of the Augusta graben, but are observed also on the limestone outcrops of the Mt. Tauro horst. As in the Villasmundo area, a certain amount of horizontal deformation is expected in association to large vertical subsidence, but this phenmomena seems able to explain only the horizontal signal over the graben. To assume that the entire Mt.Tauro limestone horst is moving West in response to the Augusta plain subsidence would imply that the compaction occurs at greater depths (in the bedrock0) than observed. Moreover, a similar deformation pattern can be observed in the S. Maddalena limestone horst (in the SR area to the South, Fig. 1) which shares with Mt.Tauro a similar tectonic setting, flanked by NW-trending faults on either side. Not much is known on these faults, but at least the Mt. Tauro western fault is considered active on the basis of the occurrence of deep gas (H_2S and NH_3) upwelling during the 1990 Augusta earthquake (Dall'Aglio et al., 1995).

Given these similarities, the horizontal deformation rates observed on the two horsts could tentatively be related to the tectonic activity of their fault systems; further investigations are currently carried out in order to verify this hypothesis.

The subsidence anomaly located in the River Marcellino graben (Fig. 3a), corresponding to the petrochemical complex of Priolo-Gargallo, shows values that span from -1 mm/yr to -5 mm/yr. The largest subsidence values are located near the river Marcellino and a large mineral-oil tank. In this case, the subsidence is mainly due to industrial groundwater overdraft. In the area 16 wells are pumping on average 13.000 m^3/day (URS corporation, 2003) for industrial supply and the interference phenomena between the several cones of depression has produced a general condition of overexploitation in the lower aquifer. The stratigraphic column n°4 reported by the 1:50.000 Geologic map – (Lentini *et al.*, 1986) located 400 meters North of the River Marcellino mouth reports ~10 meters of silty-clay of lagoon environment, lying above the Plio-Pleistocene volcanites. These sediments belong to the soft basal member of the lower-Pleistocene calcarenites (Qc, fig. 2) and hence could represent the best candidate for the compaction source. The horizontal velocity component in this case appears very noisy and does not reveal any distinguishable trend, showing very small deformation rates, mostly comprised within the uncertainties (Fig. 3b).

The subsidence ongoing west of Siracusa (Fig. 3a) is sited in a low-lying reclaimed area and is located near a well field and another industrial complex; water table lowering has also been reported here

(Lentini *et al.*, 1986). The measured Up velocity values reach -6 mm/yr, along the coastal strip. In this case, the occurrence of subsidence is particularly critical for its relevance to flooding hazards. The Siracusa Civil Protection (Arnone and Lucchesi, 2005) describe this lowland alluvial plain as flood prone because the seaward drainage rate of meteoric water is rather slow, even after moderate rainfalls. This has been attributed to the lack of maintenance and consequent deterioration and obstruction of the drainage channels by sediment and vegetation (Arnone and Lucchesi, 2005). The same area is also subjected to flood hazard from the Anapo river (Arnone and Lucchesi, 2005), and has been classified as a high to very high risk zone, due to the presence of many vulnerable infrastructures (railways, streets, factories and well fields). Land subsidence, especially along the coast, has surely worsened the problem. Subsidence-induced damages include the loss of altitude of the ground and loss of the ability of flood-control and drainage projects to prevent flooding, loss of freeboard of bridges and conveyance capacities of inland rivers. Based on the present rates and on the age of the causative factors we can hypothesize a cumulative ground lowering of several decimeters in the last 50 years. A practical example of the negative influence of subsidence on drainage rates in this area is shown by the forced diversion of two channels located in the highest deformation area, towards another channel, where smaller deformation rates are measured (Arnone and Lucchesi, 2005).

In the SR case, land subsidence may be attributed to intensive groundwater pumping from the lower aquifer, but there is probably a minor component due to compaction of fine sediment and backfilling material triggered by artificial drainage, and decomposition of organic material. These lands, such as many others along the Ionian coast, were reclaimed by drainage at the beginning of the last century (URL: http://seby4474.interfree.it/wwf2003/ciane02.htm), and certainly compaction has been active for many years after reclamation. Bennema et al. (1954), reported that clay deposits containing 30-35 % of a less-than 2-micrometer particle-size fraction (fine) compressed to about 50% of their original thickness after reclamation over a 100-year period, while sediments with 20% fine fraction compressed about 25%. In this sector, the East ground velocity component shows small negative values in correspondence of the subsiding areas, which are interpreted as minor horizontal ground deformation triggered by the subsidence phenomena.

The circular subsidence pattern located near the village of Villasmundo differs from the others discussed above. In fact, it is not located inside a coastal graben but is sited inland, on the Hyblean plateau. The stratigraphy here is represented by the 185 m thick Plio-Pleistocene basalts, lying over the volcanoclastic rocks of the Carlentini formation (Tortonian), typically 80 to 100 meters thick, and the

basal Meso-Cenozoic carbonate succession. In this area a large number of wells up to 300 m deep, extract notable amounts of water from the volcanic (Pv), calcareous and calcarenitic (M) units of the lower aquifer to supply a public aqueduct. The deformation detected is attributed to acquifer-system compaction, and the likely candidate where compaction occurs seems to be the Carlentini formation, which is mainly composed of granular deposits, although it may contain few-meter thick compressible clay layers, derived from the alteration of volcanoclastic rocks (Bandieri and Pizzarotti, 2008, table no.2).

The circular subsidence pattern is not well matched by the distribution of the wells (active or exhausted, see Fig. 4) which are all located east of the maximum subsidence of -5 mm/yr. Most of these wells produce from basal carbonates with water yields up to 20 l/s.

By analyzing the relative trends of the vertical and the horizontal components of the deformation, we can derive further useful information. Going from West to East, the East velocity over the subsiding area gradually increases up to 2.3 mm/yr, then decreases to -2.2 mm/yr and then tends to return to zero far from the subsidence area (Fig. 4). The change of sign occurs in the area of the maximum vertical deformation. This pattern indicates that for a radius of at least 1 km around the maximum subsidence area, the ground is moving, with significant horizontal velocities, towards the centre of the subsidence bowl.

The occurrence of horizontal deformation in subsidence areas has been noted elsewhere (e.g. Bawden *et al.*, 2001; Watson *et al.*, 2002; King *et al.*, 2007), but where permanent subsidence attributed to inelastic deformation is occurring, horizontal deformation is usually only a small fraction of the vertical deformation (Hoffmann and Zebcker, 2003). Where recoverable subsidence attributed to elastic deformation is occurring, horizontal deformation may be a relatively large fraction of the vertical deformation (Burbey and Helm, 1999). We have no precise information on the amount of acquifer depletion during the period considered here, and very coarse knowledge of the geomechanical properties of the aquifer units. Therefore, we do not attempt to model the deformation signal using numerical or analytical approaches based on the consolidation and poroelasticity theories (Burbey and Helm, 1999).

Instead, we assume that the observed DInSAR ground velocity patterns may result mainly from elastic deformation of the Plio-Pleistocene basalts, driven by compaction of the layers underneath. In fact, using a simple model simulation of the surface deformation caused by a shallow planar contracting zone embedded in an elastic, homogeneous half space (Okada, 1985) we obtain patterns of vertical and E-W deformation (Fig. 8) very similar to the observed ones (Fig. 9).

Under the previous assumption, we attempt an inversion modelling of our observations in the Villasmundo area, to study the geometry and depth of the layers affected by effective stress increase due to hydraulic head decline.

We use a two-step procedure involving non-linear and linear data inversion (see Atzori *et al.*, 2008), and the Okada (1985) formulations (Watson *et al.,* 2002; Fielding *et al.,* 1998), to solve for the depth of the horizontal compacting layer and for the spatial distribution of compaction values. Our final model shows a very good fit to the ascending and descending observations (Fig. 10) yielding RMS of residuals of 0.5 mm/yr, and 0.5 mm/yr respectively. According to such approximated model, the compacting layer is located at ~250 m depth, which is in agreement with the hypothesis that compaction occurs in the Carlentini formation, caused by lowering of the hydraulic head. The non-coincidence between well location and maximum surface deformation is not accounted for by our simple model, and may arise from lateral and vertical lithologic variations in the stratigraphic column, perhaps due to local Quaternary faults (Fig. 10).

Finally, we note that for the Augusta subsidence area the same procedure cannot be used. Here the ratio between vertical and horizontal velocities does not reproduce the typical signature in Fig. 8, and shows instead a very noisy trend. This supports the interpretation that in this area inelastic deformation mechanisms presently dominate.

Conclusions

The development of industrialization and intensive agriculture along the Ionian coast of southeastern Sicily, and the consequent urbanization, led to the exploitation of groundwater resources at accelerated rates, in order to meet the water demands of increasing population and industrial expansion. This trend, compromised the precarious balance between groundwater recharge and discharge, leading to groundwater depletion, aquifer-system compaction and land subsidence, especially in the areas where soft Quaternary sediments cap the deep aquifer system or are interbedded in the upper aquifer.

In the Augusta area, the presence of subsidence has been hypothesized since the 1980s, when the overexploitation of the aquifer increased dramatically. However, no long-term monitoring strategies have ever been devised, and there has been no quantitative assessment of ground deformation up to this study. There is also a general lack of piezometric time series, which prevents a direct correlation of the subsidence trends to the groundwater-level fluctuations through time and space. However, the good spatial and temporal resolution, and the 8-year long time series of the DInSAR observations allow a clear separation of local, high spatial frequency subsidence patterns due to more superficial causes (soil

consolidation due to recent engineering construction), from smoother, lower spatial frequency patterns due to the long-term compaction of sediment layers at depth. The hydrogeological setting of the Augusta basin, the long history of pumping, and the large vertical/horizontal velocity ratio suggest that the present ground subsidence is mostly driven by inelastic compaction of the fine grained deposits, which could not be recovered in case of aquifer recharge.

In addition to significant reduction of aquifer storativity, the occurrence of unrecoverable subsidence in such a low lying coastal areas can lead to many other collateral effects: flooding, inundation, overflow, saline intrusion, differential settlements and damage to engineering structures, differential changes in elevation and gradient of stream channels, drains and water-transport structures. Moreover, the emplacement of decontamination works as well points and hydraulic barriers, scheduled for the next years in the petrochemical complex of Augusta-Priolo could worsen the situation in the long-term.

We were able to measure, also for the first time, considerable subsidence around the Villasmundo public well field. Here too there was a lack of geodetic monitoring, stratigraphic and piezometric level data. However, using an analysis supported by a simple modeling approach, we suggest that elastic compaction occurring at about 250 m depth is the dominant deformation mechanism in this case.

Finally, we stress that, even if multi-temporal DInSAR techniques have proved to be very effective for the monitoring of past and present subsidence, in order to adequately describe the phenomena and analyze all possible implications arising in such highly vulnerable areas, a large effort must be made to ensure continuous, long-term monitoring of surface deformation and hydrogeological parameters.

Acknowledgements

We thank R. Lanari, at IREA-CNR, Naples, for providing the SBAS software for the SAR data processing. The ERS data are copyright of the European Space Agency, and were provided under the Category 1 project 3769. C. Tolomei has been supported by the SIGRIS project of the Italian Space Agency. We thank R. Devoti for providing the GPS site velocities. Finally, we are indebted to S. Atzori for providing software and knowledge for the elastic modeling. F. Canova has been supported by Italian Ministry of Education, University and Research scholarship (Fondo per il sostegno dei giovani).

References:

Adam J, Reuther CD, Grasso M, Torelli L. 2000. Active fault kinematics and crustal stresses along the Ionian margin of south-eastern Sicily. *Tectonophysics* **326**, 217-239.

Amelung F, Galloway DL, Bell JW, Zebker HA, Laczniak RL. 1999. Sensing the ups and downs of Las Vegas—InSAR reveals structural control of land subsidence and aquifer-system deformation: *Geology*, **27**, 483-486.

Amato A, Azzara R, Basili A, Chiarabba C, Cocco M, Di Bona M, Selvaggi G. 1995. Main shock and after shocks of the December 13, 1990 Eastern Sicily earthquake, *Ann. Geofis.*, **38**, 255-266.

Arnone G, Lucchesi T. 2005. Piano Stralcio di Bacino per l'Assetto Idrogeologico (P.A.I.). Area territoriale tra il bacino del fiume San Leonardo ed il Bacino del fiume Anapo (092). URL: http://www.sitr.regione.sicilia.it/pai/bac092.htm

Atzori S, Manunta M, Fornaro G, Ganas A, Salvi S. 2008. Postseismic displacement of the 1999 Athens earthquake retrieved by the Differential Interferometry by Synthetic Aperture Radar time series, *J. Geophys. Res.*, **113**, B09309, doi:10.1029/2007JB005504.

Aureli A, Chiavetta A. 1985. Tridimensional and paleogeographical riconstruction of an aquifer submitted to overexploitation and in danger of subsidence. *Scheme for mathematical model. V International symposium on ground water*, Taormina, 17-21 Nov. 1985.

Aureli A, Adorni G, Chiavetta AF, Fazio F, Fazzina S, Messineo G. 1987a. Carta Idrogeologica di una regione ove sono presenti acquiferi sovrasfruttati. *Mem. Soc. Geol. It.* **37**, 27-34, 4 ff,

Aureli A, Adorni G, Chiavetta AF, Fazio F, Fazzina S. 1987b. Caratteristiche delle linee di flusso dell'intrusione marina influenzate dalla tettonica in area costiera ove gli acquiferi sono sovrasfruttati. *Mem. Soc. Geol. It.* **37**, 481-488, 7 ff.

Aureli A, Adorni G, Chiavetta AF, Fazio F. 1987c. Condizioni di vulnerabilità di acquiferi in zona a forte insediamento industriale di tipo petrolchimico. *Mem. Soc. Geol. It.* **37**, 35-52, 11 ff.

Baek J, Kim SW, Park HJ, Jung HS, Kim KD, Kim JW. 2008. Analysis of ground subsidence in coal mining areas using SAR interferometry. *Geosciences Journal*, **12**, n. 3, 277-284, DOI: 10.1007/sl2303-008-0028-3.

Bandieri S, Pizzarotti MP. 2008. Le gallerie naturali della Catania-Siracusa. *Le strade*, 9/2008, pp 64-74, casa editrice la Fiaccola srl.

Baratta M. 1901. I Terremoti d'Italia, Arnaldo Forni, Bologna.

Barends F, Brouwer F, Schröder, F. 1995. Land Subsidence, Balkema, Rotterdam, The Netherlands (ISBN 90 5410 589 5), ppXI-XIV.

Formattato: Italiano (Italia)

572 Bawden G, Thatcher W, Stein R, Hudnut K, Peltzer G. 2001, Tectonic contraction across Los Angeles
573 after removal of groundwater pumping effects, *Nature*, **412**, 812– 815.
574 Ben-Avraham Z, Grasso M. 1991. Collisional zone segmentation in Sicily and surrounding areas in the
575 central Mediterranean. *Ann Tectonicae*, **5**, 131-139.
576 Bennema J, Geuze ECWA, Skits H, Wiggers AJ. 1954. Soil compaction in relation to Quaternary
577 movements of sea level and subsidence of the land especially in the Netherlands. *Geologie En*
578 *Mijnbouw, new ser*. **16**, no. 6, 173-178.
579 Berardino P, Fornaro G, Lanari R, Sansosti E. 2002. A new algorithm for surface deformation
580 monitoring based on small baseline differential SAR interferograms. *IEEE Trans. Geosci.*
581 *Remote Sens.* **40**, 2375-2383.
582 Bianca M, Monaco C, Tortorici L, Cernobori L. 1999. Quaternary normal faulting in south-eastern
583 Sicily (Italy): a seismic source for the 1693 large earthquake. *Geophys. J. Int.* **139**, 370-394.
584 Bianchi F, Carbone S, Grasso M, Invernizzi G, Lentini F, Longaretti G, Merlini S, Mostardini F. 1987.
585 Sicilia Orientale: profilo geologico Nebrodi-Iblei. *Mem. Soc. Geol. It.* **38**, 429-458, 8 ff., 1 tav.
586 f.t.
587 Blanco-Sanchez P, Mallorquí JJ, Duque S, Monells D. 2008. The Coherent Pixels Technique CPT): An
588 Advanced DInSAR Technique for Nonlinear Deformation Monitoring. *Pure Appl. Geophys.*, No.
589 165, pp. 1167-1194.
590 Borgia A, Tizzani P, Solaro G, Manzo M, Casu F, Luongo G, Pepe A, Berardino P, Fornaro G,
591 Sansosti E, Ricciardi GP, Fusi N, Di Donna G, Lanari R. 2005. Volcanic spreading of Vesuvius,
592 a new paradigm for interpreting its volcanic activity. *Geophys. Res. Lett.* **32**, L03303, doi:
593 10.1029/2004GL022155.
594 Burbey TJ, Helm DC. 1999. Modeling three-dimensional deformation in response to pumping of
595 unconsolidated aquifers. *Environ. Eng. Geosci.*, **5**(2), 199–212.
596 Bürgmann R, Rosen PA, Fielding EJ. 2000. Synthetic aperture radar interferometry to measure earth's
597 surface topography and its deformation. *Annu. Rev. Earth Planet. Sci.* 2000. **28**:169-209.
598 Carbone S. 1985. I depositi pleistocenici del settore nord-orientale ibleo tra Agnone e Melilli (Sicilia
599 SE): relazione tra facies e lineamenti strutturali. *Boll. Soc. Geol. It.*, **104**, 405-420, 3 ff., 1 tab., 3
600 tav.
601 Cascini L, Ferlisi S, Fornaro G, Lanari R, Peduto D, Zeni, G. 2006. Subsidence monitoring in Sarno
602 urban area via multi-temporal DInSAR technique. *Internat. J. Remote Sensing* **27**(8), 1709 1716.

Formattato: Italiano (Italia)

Formattato: Italiano (Italia)

Formattato: Italiano (Italia)

Castañeda C, Gutiérrez F, Manunta M, Galve JP. 2009. DInSAR measurements of ground deformation by sinkholes, mining subsidence, and landslide, Ebro River, Spain. *Earth Sur. Process. Landforms* **34**, 1562-1574, doi:10.1002/esp.1848

Casu F, Manzo M, Lanari R. 2006. A quantitative assessment of the SBAS algorithm performance for surface deformation retrieval. *Remote Sensing of Environ.* **102**(3–4), 195–210, doi:10.1016/j.rse.2006.01.023.

Casu F, Manzo M, Pepe A, Lanari R. 2008. SBAS-DInSAR analysis of very extended areas: First results on a 60,000 km^2 test site. *IEEE Geosci. Remote Sens. Lett.*, **5**, 438–442.

Dall'Aglio M, Quattrocchi F, Tersigni S. 1995. Geochemical evolution of groundwater of the Iblean Foreland (Southeastern Sicily) after the December 13, 1990 earthquake (M = 5.4). *Annals of Geophysics*, **38**, 2, 309-329.

Decanini L, Panza GF. 2000. Scenari di pericolosità sismica ad Augusta, Siracusa e Noto. CNR - Gruppo Nazionale per la Difesa dai Terremoti – Roma, 2000, 200 pp.

Devoti R, Pietrantonio G, Pisani AR, Riguzzi F, Serpelloni E. 2010. Present day kinematics of Italy. *Journal of the Virtual Explorer, Electronic Edition*, ISSN 1441-8142, volume 36, paper 2. In: (Eds.) Marco Beltrando, Angelo Peccerillo, Massimo Mattei, Sandro Conticelli, and Carlo Doglioni, The Geology of Italy, 2010.

DISS Working Group. 2010. Database of Individual Seismogenic Sources (DISS), Version 3.1.1: A compilation of potential sources for earthquakes larger than M 5.5 in Italy and surrounding areas. Available at http://diss.rm.ingv.it/diss/, © INGV 2010 - Istituto Nazionale di Geofisica e Vulcanologia - All rights reserved.

Dziewonski A, Bloch S, Landisman M. 1969. A Tecnique for the Analysis of Transient Seismic Signals. *Bull.Seism.Soc.Am.*, **59**, pp.427-444.

Ferretti A, Prati C, Rocca F. 2001. Permanent Scatterers in SAR Interferometry. *IEEE Trans. Geoscience And Remote Sensing*, **39**(1), 8–20.

Fielding E, Blom R, Goldstein R. 1998. Rapid subsidence over oil fields measured by SAR interferometry. *Geophys. Res. Lett.*, **25**(17), 3215 – 3218.

Figueroa-Vega GE. 1984. Case history no. 9.8. Mexico., D. F., Mexico, in Poland, J.F. ed., Guidebook to studies of land subsidence due to ground-water withdrawal. United Nations Educational, Scientific and Cultural Organization, Paris, Studies and reports in hydrology 40, p. 217–232, http://wwwrcamnl.wr.usgs.gov/rgws/Unesco/, accessed November 28, 2007.

Formattato: Italiano (Italia)

Formattato: Italiano (Italia)

634 Franceschetti G, Lanari R. 1999. Synthetic Apertyre Radar Processing (CRC Press, Boca Raton FL
635 1999)
636 Galloway DL, Hoffmann J. 2007. The application of satellite differential SAR interferometry-derived
637 ground displacements in hydrogeology. *Hydrogeology Journal*, v. **15** (1), p. 133-154. DOI
638 10.1007/s10040-006-0121-5.
639 Galloway DL, Jones DR, Ingebritsen SE. 1999. Land subsidence in the United States: U.S. Geological
640 Survey Circular 1182, 177 p.[http://pubs.usgs.gov/circ/circ1182/]
641 Galloway DL, Hudnut KW, Ingebritsen SE, Phillips SP, Peltzer G, Rogez F, Rosen PA. 1998.
642 Detection of aquifer system compaction and land subsidence using interferometric synthetic
643 aperture radar, Antelope Valley, Mojave Desert, California. *Water resources research*, vol. 34,
644 NO. 10, 2573-2585, October 1998.
645 Ghisetti F, Vezzani L. 1980. The structural features of the Iblean Plateau and of the Monte Judica area
646 (south-eastern Sicily): a microtectonic contribution to the deformational history of the Calabrian
647 Arc. *Boll. Soc. Geol. It.* **99**, 57-102.
648 Grasso M. 1993. Pleistocene structures along the Ionian side of the Hyblean Plateau (SE Sicily):
649 implications for the tectonic evolution of the Malta Escarpment. In: Max, M.D., Colantoni, P.
650 (Eds), Geological Development of the Sicilian-Tunisian Platform. *UNESCO reports in Marine*
651 *Science* **58**, 49-54.
652 Guzzetti F, Manunta M, Ardizzone F, Pepe A, Cardinali M, Zeni G, Reichenbach P, Lanari R. 2009.
653 Analysis of Ground Deformation Detected Using the SBAS-DInSAR Technique in Umbria,
654 Central Italy. *Pure appl. Geophys.* **166**, 1425-1459. 0033–4553/09/081425–35, DOI
655 10.1007/s00024-009-0491-4
656 Hoffmann J, Galloway DL, Zebker HA. 2003, Inverse modeling of interbed storage parameters using
657 land subsidence observations, Antelope Valley, California. *Water-Resources Research*, v. **39** (2),
658 doi: 10.1029/2001WR001252, p. SBH 5-1 – 5-10.
659 Hoffmann J, Zebker HA. 2003, Prospecting for horizontal surface displacements in Antelope Valley,
660 California, using satellite radar interferometry. *J. Geophys. Res.*, **108**(F1), 6011,
661 doi:10.1029/2003JF000055.
662 Hooper A, Zebker H, Segall P, Kampes B. 2004. A New Method for Measuring Deformation on
663 Volcanoes and Other Natural Terrains Using InSAR Persistent Scatterers. *Geophys. Res. Letters*,
664 **31**, L23611, doi:10.1029/2004GL021737, 2004

665 Hu RL, Yue ZQ, Wang LC, Wang SJ. 2004. Review of current status and challenging issues of land
666 subsidence in China. *Eng. Geol.* **76**, 65-77.
667 Hunstad I, Pepe A, Atzori S, Tolomei C, Salvi S, Lanari R. 2009. Surface deformation in the Abruzzi
668 region, Central Italy, from multitemporal DInSAR analysis. *Geophysical Journal International,*
669 **178**: 1193–1197. doi: 10.1111/j.1365-246X.2009.04284.x
670 Jacob CE. 1940. On the flow of water in an elastic artesian aquifer. *Am. Geophys. Union Trans.*, pt. 2,
671 574-586.
672 Kim JS, Kim DJ, Kim SW, Won JS, Moon WM. 2007. Monitoring of urban land subsidence using
673 PSinSAR. *Geosciences Journal* **11**, 59-73.
674 King NE, Argus D, Langbein J, Agnew DC, Bawden G, Dollar RS, Lui Z, Galloway D, Reichard E,
675 Yong A, Webb FH, Bock Y, Stark K, Barseghian D. 2007, Space geodetic observations of
676 expansion of the San Gabriel Valley, California, aquifer system, during heavy rainfall in winter
677 2004-2005. *J. Geophys. Res.* v. **112**, B03409, doi:10.1029/2006JB004448.
678 Lanari R, Berardino P, Borgstrōm S, Del Gaudio C, De Martino P, Fornaro G, Guarino S, Ricciardi
679 GP, Sansosti E, Lundgren P. 2004a. The use of IFSAR and classical geodetic techniques for
680 caldera unrest episodes: Application to the Campi Flegrei uplift event of 2000. *J. Volcanol.*
681 *Geotherm. Res.* **133**, 247–260.
682 Lanari R, Lundgren P, Manzo M, Casu F. 2004b. Satellite radar interferometry time series analysis of
683 surface deformation for Los Angeles, California. *Geophys. Res. Lett.* **31**, L23613,
684 doi:10.1029/2004GL021294.
685 Lanari R, Mora O, Manunta M, Mallorquì JJ, Berardino P, Sansosti E. 2004c. A Small Baseline
686 Approach for Investigating Deformation on Full resolution Differential SAR Interferograms,
687 IEEE Transact. *Geoscience and Remote Sensing* **42**, 7.
688 Lanari R, Casu F, Manzo M, Zeni G, Berardino P, Manunta M, Pepe A. 2007. An Overview of the
689 small baseline subset algorithm: A DInSAR technique for surface deformation analysis. *Pure*
690 *Appl. Geophys.* **164**(4), 637–661.
691 Lentini F. 1986. Carta Geologica del settore Nord-Orientale Ibleo, scala 1:50.000. Università di
692 Catania, Istituo di Scienze della Terra. S.EL.CA., Firenze.
693 Lentini F, Grasso M, Carbone S. 1987. Introduzione alla Geologia della Sicilia e guida all'escursione.
694 *Atti Convegno Soc. Geol. It.* Naxos-Pergusa, 1-60.
695 Levshin A, Pisarenko VF, Pogrebinsky GA. 1972. On a frequency-time analysis of oscillations. *Ann.*
696 *Geophys.* **28**, fasc.2, pp.211-218.

Formattato: Italiano (Italia)

Formattato: Italiano (Italia)

Formattato: Italiano (Italia)

Lo Presti DCF, Maugeri M, Cavallaro A, Pallara O. 1998. Shear modulus and damping of a stiff marine clay from in situ and laboratory test. *Geotechnical Site Characterization*, Robertson & Mayne (eds), 1998 Balkerna, Rotterdam, ISBN 90 5410 939 4.

Lundgren P, Usai S, Sansosti E, Lanari R, Tesauro M, Fornaro G, Berardino P. 2001. Modeling surface deformation observed with synthetic aperture radar interferometry at Campi Flegrei Caldera. *J. Geophys. Res.*, **106**, 19,355-19,366, doi:10.1029/2001JB000194.

Lundgren P, Casu F, Manzo M, Pepe A, Berardino P, Sansosti E, Lanari R. 2004. Gravity and magma induced spreading of Mount Etna volcano revealed by satellite radar interferometry. *Geophys. Res. Lett.* **31**, L04602, doi:10.1029/2003GL018736.

Manzo M, Ricciardi GP, Casu F, Ventura G, Zeni G, Borgstrōm S, Berardino P, Del Gaudio C, Lanari R. 2006. Surface deformation analysis in the Ischia island (Italy) based on spaceborne radar interferometry. *J. Volcanol. Geotherm. Res.* **151**, 399–416, doi:10.1016/j.jvolgeores.2005.09.010.

Marsal RJ, Mazari M. 1959. El subsuelo de la Ciudad de México. Primer Congreso Panamericano de Mecánica de Suelos y Cimentaciones, México, D.F. Republished in 1969 with english translation.

Massonet D, Feigl KL. 1998. Radar interferometry and its application to changes in the earth's surface. *Rev. Geophys.*, **36**(4), 441-500.

Meinzer OE, Hard HA. 1925. The artesian water supply of the Dakota sandstone in North Dakota with special reference to the Edgeley quadrangle. *U.S. Geol. Survey Water-Supply Paper* 520-E, 73-95.

Mora O, Mallorqui JJ, Broquetas A. 2003. Linear and nonlinear terrain deformation maps froma reduced set of interferometric SAR images, IEEE Trans. *Geosci. Remote Sens.*, **41**, 2243–2253, doi:10.1109/TGRS.2003.814657.

Nagel NB. 2001. Compaction and subsidence Issues Within the Petroleum Industry: from Wilmington to Ekofish and Beyond. *Phis. Chem. Earth* (A), Vol. **26**, No 1-2, pp. 3-14, 2001.

Okada Y. 1985. Surface deformation due to shear and tensile faults in a half-space. *Bulletin of the Seismological Society of America*; August 1985; v. **75**; no. 4; p. 1135-1154

Panza GF. 1981. The Resolving Power of Seismic Surface Waves with respect to Crust and Upper Mantle Structural Models. In: The solution of the inverse problem in geophysical interpretation. Cassinis R. Ed. : Plenum Publishing Corporation.

Poland JF, Lofgren BE, Ireland RL, Pugh RG. 1975. Land subsidence in the San Joaquin valley as of 1972. *U.S. Geol. Survey Prof. Paper* **437-H**, 78 p.

Formattato: Italiano (Italia)

Formattato: Italiano (Italia)

Formattato: Italiano (Italia)

Formattato: Inglese (Stati Uniti)

Prati C, Ferretti A, Perissin D. 2010. Recent advances on surface ground deformation measurement by means of repeated space borne SAR observations. *J. Geodyn.*, **49**, 161–170, doi:10.1016/j.jog.2009.10.011.

Riley FS. 1969. Analysis of borehole extensometer data from central California, in Tison, L.J., ed., *Land subsidence*, Vol. 2 Internat. Assoc. Sci. Hydrology, Pub. **89**, 423-431.

Salvi S, Atzori S, Tolomei C, Allievi J, Ferretti A, Rocca F, Prati C, Stramondo S, Feuillet N. 2004. Inflation rate of the Colli Albani volcanic complex retrieved by the permanent scatterers SAR interferometry technique. *Geophys. Res. Lett.* **31** (2004), p. L12606 doi:10.1029/2004GL020253

Scandone P, Patacca E, Radoicic R, Ryan WBF, Cita MB, Rawsom M, Chezar H, Miller E, Mckenzie J, Rossi S. 1981. Mesozoic and Cenozoic rocks from Malta Escarpment (Central Mediterranenan). *Am. Assoc. Petrol. Geol. Bull.*, **65**, 1299-1319.

Schmidt DA, Bürgmann R. 2003. Time dependent land uplift and subsidence in the Santa Clara Valley, California, from a large interferometric synthetic aperture radar data set. *J. Geophys. Res.*, **108**(B9), 2416, doi:10.1029/2002JB002267.

Stramondo S, Saroli M, Tolomei C, Moro M, Doumaz F, Pesci A, Loddo F, Baldi P, Boschi E. 2007. Surface movements in Bologna (Po Plain-Italy) detected by multitemporal DInSAR. *Remote Sens. Environ.*, 110, 304 – 316.

Strozzi T, Wegmüller U, Tosi L, Bitelli G, Spreckels V. 2001. Land subsidence monitoring with differential SAR interferometry. *Photogrammetric Engineering & Remote Sensing*, **67**, pp 1261-1270.

Terzaghi K. 1925. Principles of soil mechanics: IV, Settlement and consolidation of clay. *Eng. News-Rec.*, 874-878.

Tizzani P, Berardino P, Casu F, Euillades P, Manzo M, Ricciardi GP, Zeni G, Lanari R. 2007. Surface deformation of Long Valley Caldera and Mono Basin, California, investigated with the SBAS-InSAR a p p r o a c h. *Remote Sens. Environ.,* **108**, 277-289, doi:10.1016/j.rse.2006.11.015

Torelli L, Grasso M, Mazzoldi G, Peis D. 1998. Plio-Quaternary tectonic evolution and structure of the Catania foredeep, the northern Hyblean Plateau and the Ionian shelf (SE Sicily). *Tectonophysics* **298**, 209-221.

URL: http://seby4474.interfree.it/wwf2003/ciane02.htm

Valyus VP, Keylis-Borok VI, Levshin AL. 1968. Determination of the velocity profile of the upper mantle in Europe Nauk SSSR, Vol.**185**, No.8, pp.564-567.

Formattato: Italiano (Italia)

Formattato: Italiano (Italia)

Formattato: Inglese (Stati Uniti)

761 Watson KM, Bock Y, Sandwell DT. 2002. Satellite interferometric observations of displacements
762 associated with seasonal groundwater in the Los Angeles basin. *J. Geophys. Res.*, **107**(4), 2074,
763 10.1029/2001JB000470.
764 Wegmüller U, Werner C, Strozzi T, Wiesmann A. 2004. Multi-temporal interferometric point target
765 analysis", in Analysis of Multi-temporal remote sensing images, Smits and Bruzzone (ed.), Series
766 in Remote Sensing, Vol. **3**, World Scientific (ISBN 981-238-915-61), pp. 136-144, 2004.
767 Wright TJ, Parsons BE, Lu Z. 2004. Toward mapping surface deformation in three dimensions using
768 InSAR. *Geophys. Res. Lett.*, **31**, L01607, doi:10.1029/2003GL018827.
769

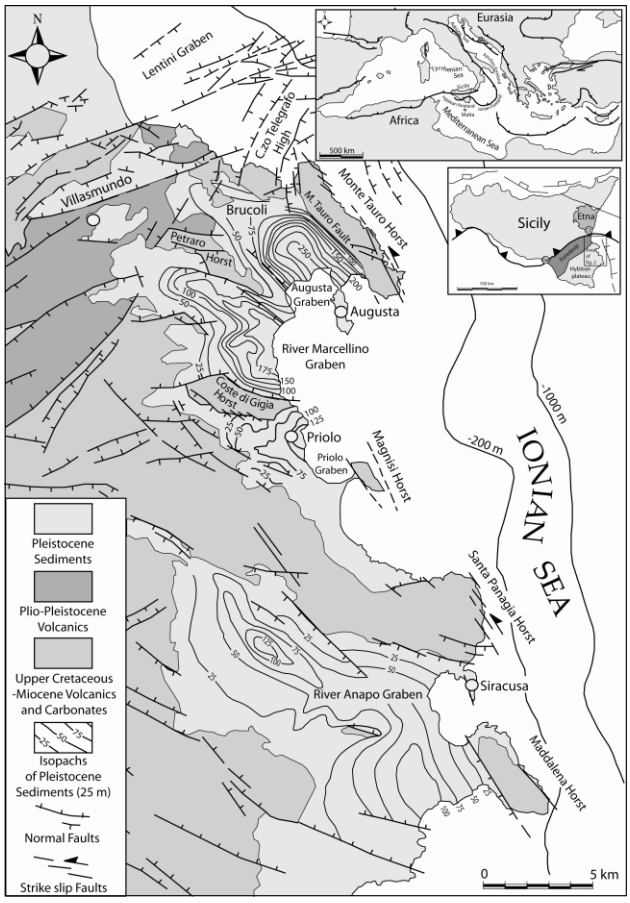

Figure 1a: Geological sketch Map of the study area (Ionian side of the Hyblean plateau, SE Sicily), redesigned after Adam et al. 2000. Contour lines represent isopachs (in meters) of Pleistocene sediments. Fig. 1b: Schematic tectonic map of the Mediterranean region showing major thrust-fold belts and strike-slip faults. HF= Hyblean foreland, IF= Ionian Foreland, AF= Apulian Foreland. Fig. 1c: Regional tectonic framework of Sicily displaying the main geologic elements. Offshore data taken from Torelli et al. (1998). HP= Hyblean plateau, E= Mount Etna. Fig 1a extent indicated by dashed box.

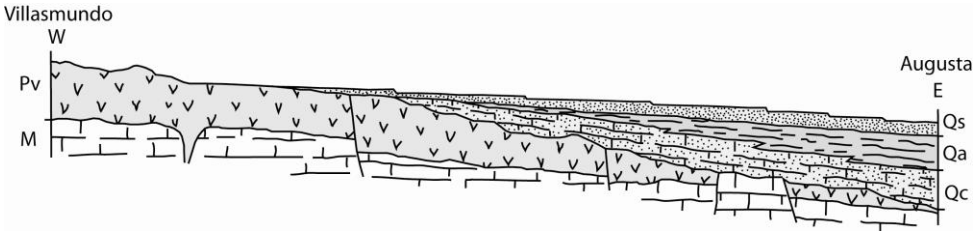

Figure 2: Schematic geological profile drawn from Villasmundo towards the sea (East), illustrating the stratigraphic relationship between Pleistocene Units and Upper Cretaceous-Miocene volcanic and calcareous bedrock. Redesigned after Carbone, 1985. M= pre-Pliocene calcareous and volcanic bedrock; Pv= Pliocene volcanics; Qc= Lower Pleistocene poligenic conglomerates, calcarenites and sand; Qa=Lower Pleistocene blue clays; Qs= middle Pleistocene yellowish biogenic calcarenites.

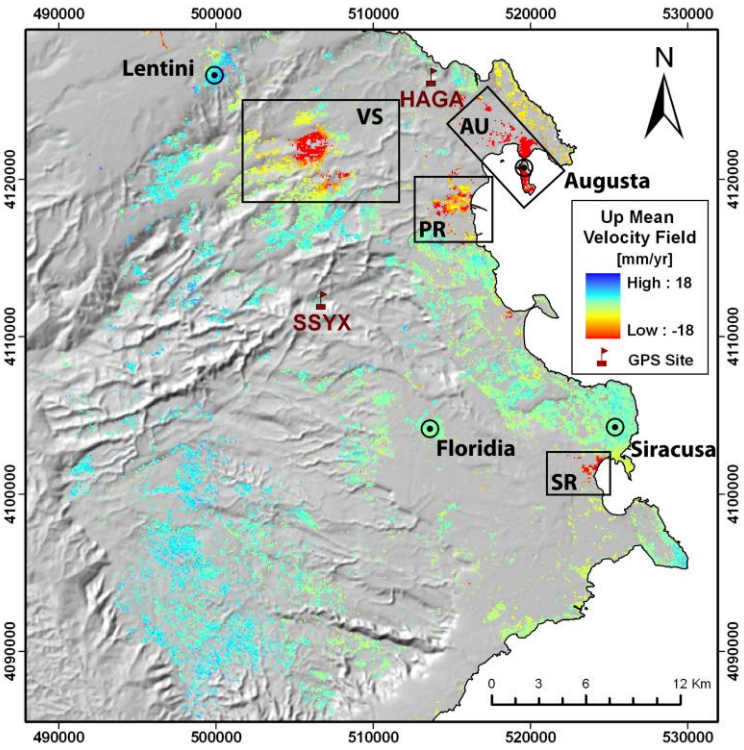

Figure 3a: Vertical ground velocities calculated using the SBAS DInSAR technique for the period 1992-2000, , overlaid on a shaded relief map of the SRTM NASA mission DEM (80x80 m)**.** Flags indicate the permanent GPS stations used to validate the data. Black boxes outline major land subsidence areas.

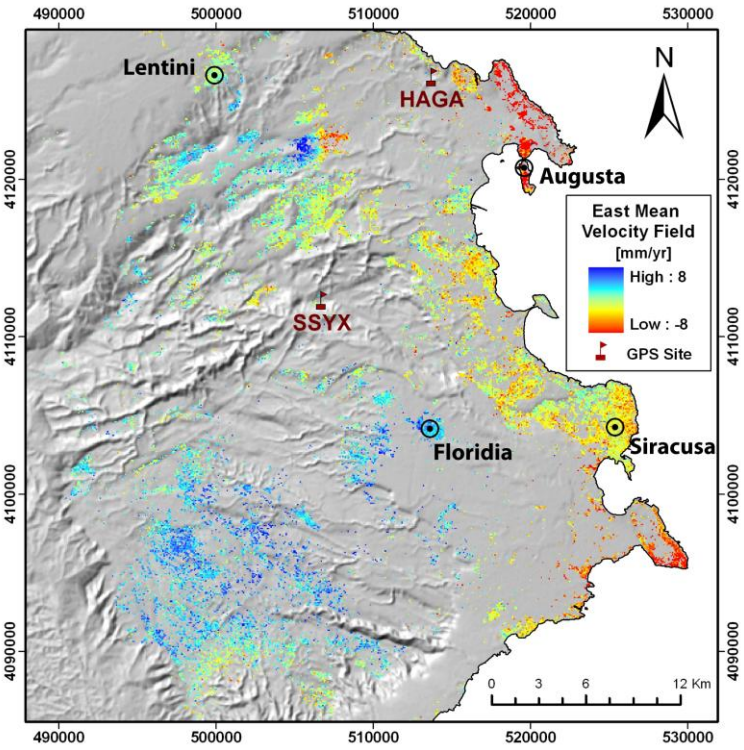

Figure 3b: East ground velocities calculated using the SBAS DInSAR technique for the period 1992-2000. Shaded relief base and symbols as in Figure 3a.

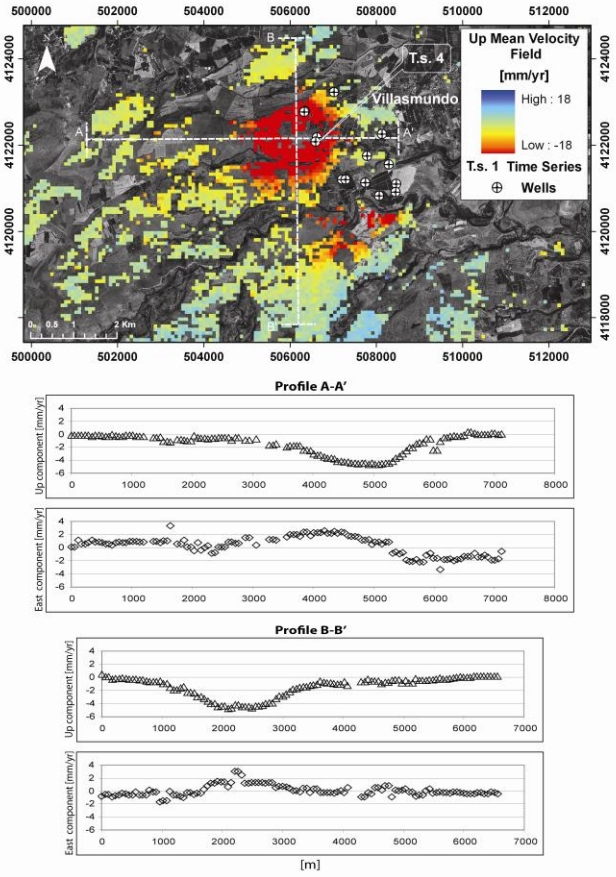

Figure 4: Vertical ground velocities for the Villasmundo site overlying an aerial photo. The location of the velocity profiles, of the time series shown in Figure 6, and of the wells of the municipal aqueduct, are reported. Lower figure shows the Up and East velocities along the profiles A-A' and B-B'.

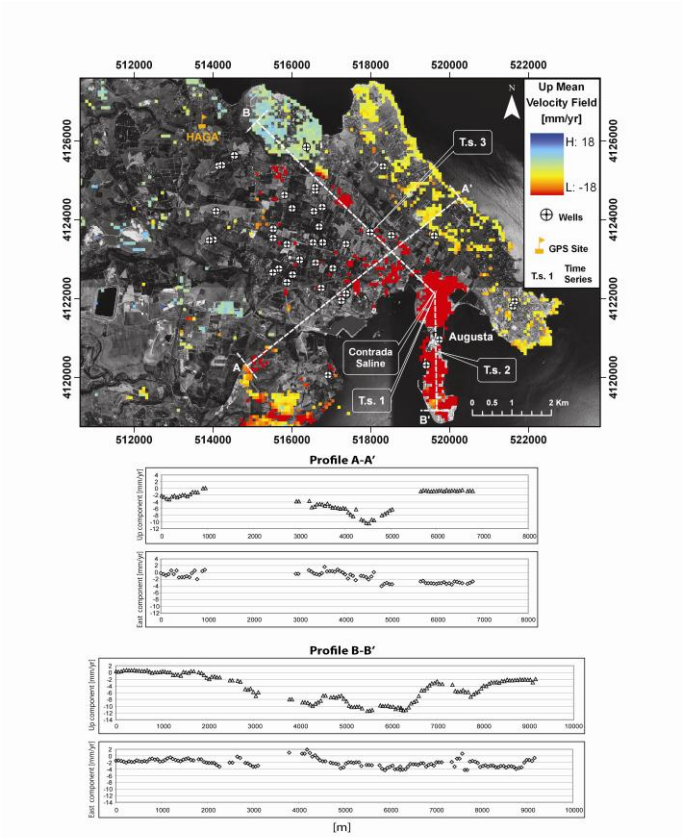

Figure 5: Vertical ground velocities for the Augusta graben area, overlying an aerial photo. The location of the velocity profiles, of the time series shown in Figure 6, and of the wells for aqueduct and agricultural use, are reported. Lower figure shows the Up and East velocities along the profiles A-A' and B-B'.

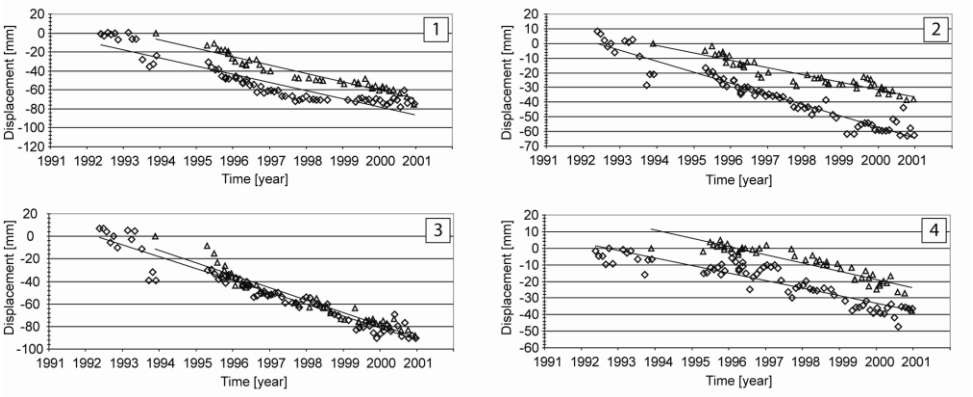

Figure 6: Time series of the ascending (triangles) and descending (diamonds) ground displacements calculated using the SBAS DInSAR technique over the period 1992-2000. T.s. n°1 has been sampled in the Contrada Saline area, and shows the effect of aquifer depletion and engineering structure loading. T.s. n°2 has been sampled over the old city of Augusta, and shows compaction due to aquifer overdraft. T.s. n°3 has been sampled in the Augusta graben area, in a not developed area, and shows subsidence due to aquifer compaction. T.s. n° 4 shows deformation ongoing in the Villasmundo area.

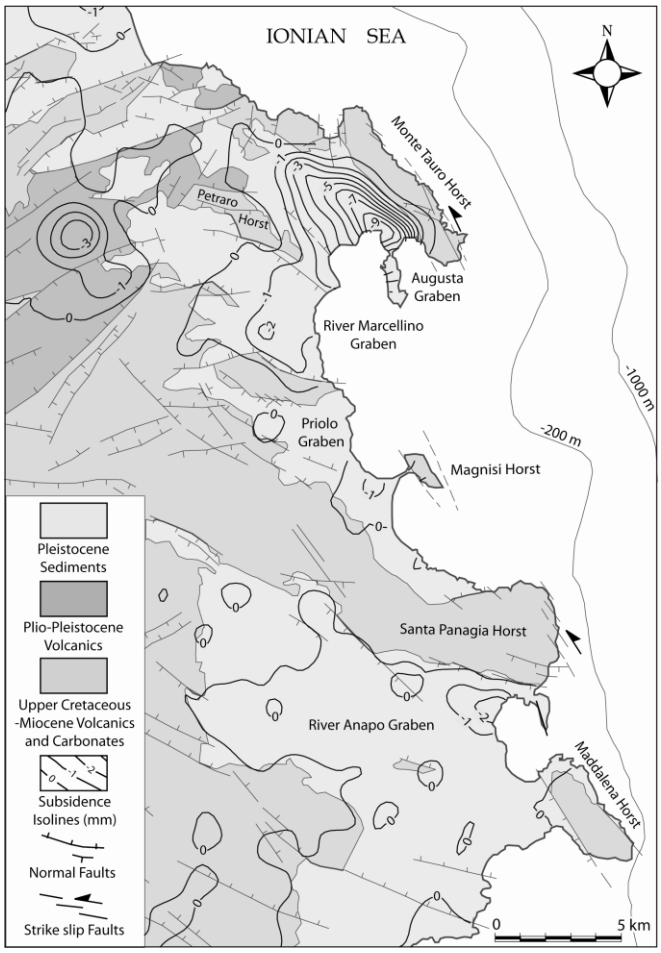

Figure 7: Contour map of subsidence rates derived from kriging interpolation, overlying a simplified geological map, in order to highlight the correspondence between subsiding areas and Quaternary deposits.

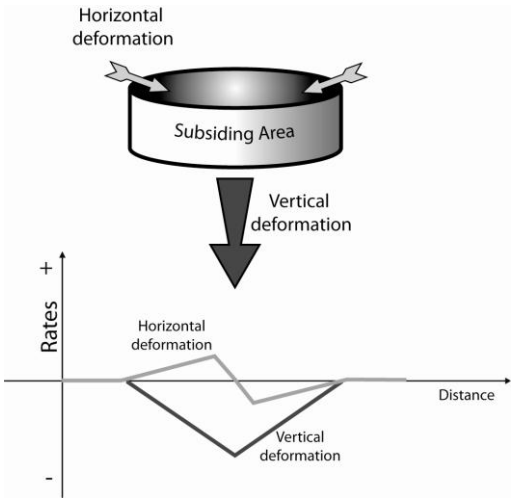

Figure 8: Upper figure: conceptual model of the deformation occurring over a symmetrical, circular subsiding area, in which surface displacement is attributed to shallow elastic deformation. Lower figure: schematic representation of vertical and horizontal deformation rates, and vertical/horizontal ratio, occurring for such a model on an E-W profile. Compare the synthetic profiles with those obtained from the SBAS velocities shown in Figure 9.

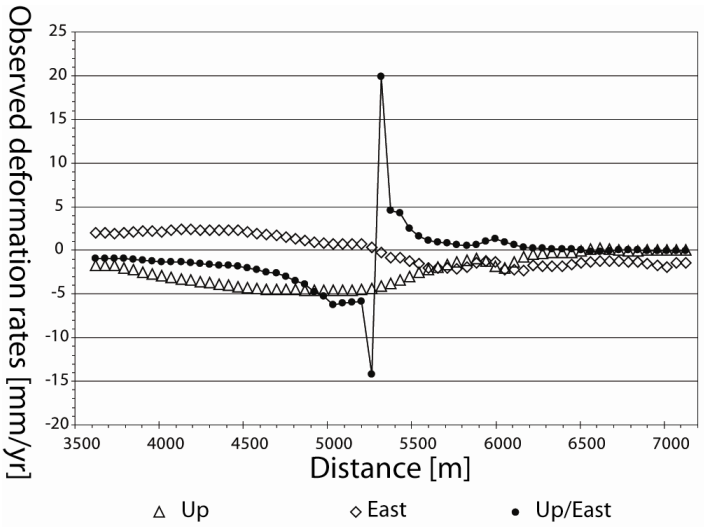

828

829 **Figure 9**: Villasmundo area: vertical and horizontal deformation rates, and vertical/horizontal ratio of
830 the SBAS DInSAR mean velocities sampled along the EW profile reported in Fig. 4. The peculiar
831 surface deformation signature caused by a planar contracting zone placed at shallow depth within an
832 elastic medium, can be observed.

833

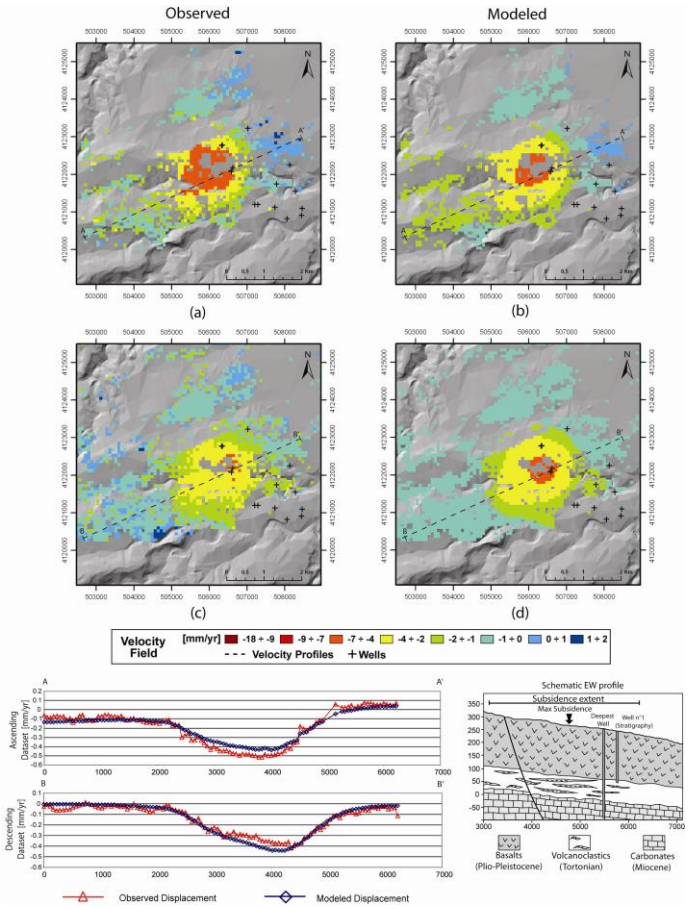

Figure 10: a) Ascending observed deformation rates b) Ascending modeled deformation rates c) Descending observed deformation rates d) Descending modeled deformation rates. Velocity profiles show the comparison between observed (red) and modeled (blue) Ascending and Descending deformation rates. A schematic EW geological profile is reported, showing our interpretation of the Villasmundo subsidence.